Crystal Orientation of Iron Produced by Electrodeoxidation of Hematite Particles

M. Tokushige[a], O.E. Kongstein[b], and G.M. Haarberg[a]

[a] Department of Materials Science and Engineering,
Norwegian University of Science and Technology,
Trondheim, NO-7491, Norway
[b] Department of Applied Mechanics and Corrosion,
Division of Materials and Chemistry, SINTEF,
Trondheim, NO-7465, Norway

Electrowinning of iron was conducted in a 50-*wt*% NaOH-H_2O electrolyte suspended Fe_2O_3 particle at 110ºC and pure α-Fe films were obtained on a disk cathode with a higher current efficiency than 95%. The Fe_2O_3 particle was directly reduced on the surface of the disk cathode and the deposited Fe atoms formed a cubic particle with a side length of approximately 0.1 μm. The crystal orientation of α-Fe depends on electrolysis conditions, such as current density and Fe_2O_3 particle concentration, and the (211) face plane of α-Fe was preferentially orientated. Therefore, a cubic α-Fe particle columnar-grows (grows in columnar formation) toward the (211) face direction by spiral dislocation after two-dimensional nucleation. Furthermore, the morphology of the obtained α-Fe film can be controlled by the current density and the transfer rate of the Fe_2O_3 particle.

1. Introduction

Iron has been used as a fundamental material. Currently, this structural material is also absolutely imperative in various fields, such as architecture, vehicle, and aircraft. However, due to the recent concern over the influence of CO_2 emissions on global warming, the low CO_2 emission industrial technology is required. The production of iron and steel in particular causes large emissions of CO_2 [1-3].

Against such a background, electrowinning in an aqueous electrolyte containing suspended Fe_2O_3 particles is an alternative process to reduce or eliminate the formation of CO_2 [2, 3]. As shown in Figure 1, the Fe_2O_3 particle suspended in the electrolyte is directly reduced by the reaction (1) and the metallic Fe phase is obtained on the surface of a rotating disk cathode [1-4].

$$Fe_2O_3 + 3H_2O + 6e^- \rightarrow 2Fe + 3OH^- \qquad [1]$$

In this process, as shown in Figure 2 [5], the cathode limit of the electrolyte (H_2 evolution) is shifted to a negative potential using a strong alkaline electrolyte so that electrowinning of iron can be conducted. The anodic reaction is the oxygen evolution. Boyan *et al*. [2] obtained an Fe film with current efficiency higher than 90% after terminating electrowinning and discovered that the morphology of the obtained Fe film changed as a result of electrolysis conditions such as the current density and the rotation speed of the disk cathode. As for the morphology of the electrodeposited Fe films, many investigations have been conducted on the electrolyte containing the dissolved iron ion and it was found that the electrodeposited Fe columnar-grows (grows in a columnar

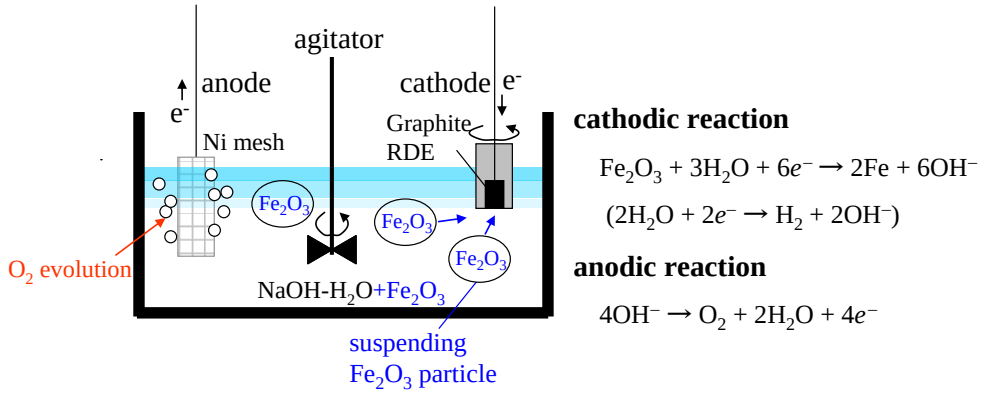

Fig. 1 Principle of iron electrowinning.

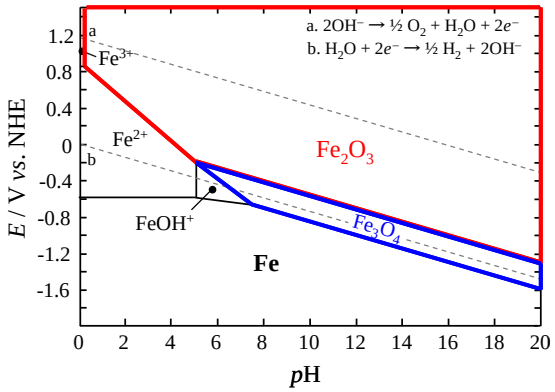

Fig. 2 Pourbaix diagram for Fe-H_2O system at110ºC [5].

formation) and its morphology changes from tetragonal to trigonal pyramids as a result of electrolysis conditions such as the current density [6-8], the pH value of the electrolyte [6-8, 15], and the applied magnetic field [9-11]. It was suggested that the nucleated Fe grew by spiral dislocation according to the two-dimensional nucleation theory [8, 14]. The formation of heterogeneous film decreases current efficiency. Therefore, in order to industrialize this process as a novel iron production method, it is necessary to clarify and control the reduction process of the Fe_2O_3 particle and the growth process of the deposited Fe, and to obtain a homogeneous Fe film.

In this study, the direct reduction of Fe_2O_3 was conducted using Fe_2O_3 pellet and the electrochemical behavior of Fe_2O_3 particle suspended in the electrolyte was investigated. Then, to determine the appropriate conditions for obtaining Fe film with homogenous morphology, the authors investigated the relation between the morphology of the obtained Fe and electrolysis conditions such as current density, rotation speed of the disk cathode, and Fe_2O_3 particle concentration.

2. Experiment

Figure 3a shows the experimental setup used in this study. Electrowinning was conducted in a 50-*wt*% (18 M) NaOH-H_2O system (NaOH: 99.0% purity, VWR International, Ltd.) containing Fe_2O_3 particle (electrolyte) at 110ºC. As shown in Figure 3b, α-Fe_2O_3 particles (hematite: 99.5% purity, 325 mesh, Alfa Aesar Gmbh & Co KG) with diameters of less than 0.2 μm were used as suspension. Electrolysis was conducted using a three-electrode

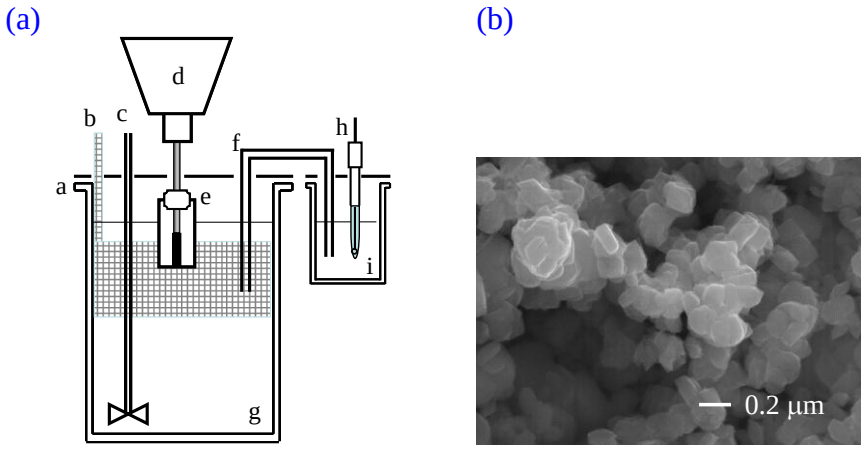

Fig. 3 (a) Schematic drawing of the experimental setup and (b) a SEM image of the α-Fe_2O_3 particle.
a. Teflon holder, b. Ni mesh (anode), c. agitator, d. motor, e. graphite disk (cathode), f. salt bridge, g. 50 *wt*% (18 M) NaOH-H_2O+Fe_2O_3 electrolyte, h. HgO/Hg reference electrode, and i. 0.1 M NaOH-H_2O reference solution

type cell. A graphite disk (ø8.0 mm) was used as a working electrode (cathode) and a Ni mesh (45×125 mm, 0.1 mm^t) was used as a counter electrode (anode). The reference electrode was a HgO/Hg electrode immersing the 1.0 M NaOH-H_2O reference solution and the salt bridge was connected between the electrolyte and the reference solution. All potential values were calibrated based on that of dynamic hydrogen electrode (DHE), where hydrogen evolution starts on Pt wire cathode. Electrochemical measurement was performed using an electrochemical measurement system (Zahner IM6, Germany).

The obtained films were dipped into a distilled water and ethanol solution thereafter, to remove the electrolyte, and were characterized by X-ray diffraction (XRD; Siemens, Bruker-AXS D5005) and field emission scanning electron microscopy (FE-SEM; Hitachi High-Technologies Corp., SU-6600).

To evaluate the crystal orientation of the deposited iron, orientation index *M* was calculated as follows:

$$M(hkl) = \frac{\dfrac{I(hkl)}{\sum I(h'k'l')}}{\dfrac{I_0(hkl)}{\sum I_0(h'k'l')}}, \qquad [2]$$

where I (hkl) is the XRD intensity of the experimental data, I_0 (hkl) is the XRD intensity in the JCPDS (Joint Committee on Powder Diffraction Standards) cards, and ΣI ($h'k'l'$) is the sum of the intensity of (110), (200) and (211). The average grain size of α-Fe crystal was estimated using Scherrer's Eq. (Eq. (3)).

$$G = \frac{0.88\,\lambda\,(\mathrm{Cu}K_\alpha)}{\beta_{2\theta}\,\cos\theta_{\max}} \qquad [3]$$

where λ (CuK_α) is the wavelength of the X-ray (0.15418 nm), $\theta_{\max}$ is the angle at the peak maximum, and $\beta_{2\theta}$ is the peak's width (in rad.) at half height.

3. Results and Discussion

3.1 Direct Reduction of Oxide Pellet

In order to confirm the direct reduction of Fe_2O_3 in 50 *wt*% NaOH-H_2O electrolyte at 110°C, the electrowinning (1.0 A, 20,000 C) was conducted using Fe_2O_3 pellet (Fig. 4a) as a cathode. Fe_2O_3 pellet was sintered at 800°C for 8 hrs. At the early stage of the electrowinning (~1.0 hr in Fig. 5a), the cathodic potential was unstable and negative values, and the hydrogen was frequently evolved. After 1.0 hr of the electrowinning, the cathodic potential became to be stable values. This is caused by the generation and expansion of Fe phase on the oxide pellet.

As shown in Figs. 4 a-c, the metallic phase appeared and expanded on the surface of the pellet by the electrolysis. An XRD pattern of the pellet after terminating electrowinning (Fig. 5b) shows that Fe_2O_3 pellet was directly reduced to metallic α-Fe phase. Here, as shown in Fig. 6, the powder obtained after terminating electrowinning (0.6 A, 100,000 C) contains Fe, Fe_2O_3 and Fe_3O_4, which confirmed that the reduction of the Fe_2O_3 proceeds by two step reactions as follows.

$$3Fe_2O_3 + e^- \rightarrow 2Fe_3O_4\ (2FeO+2Fe_2O_3) + O^{2-} \quad [4]$$

$$Fe_3O_4 + 2e^- \rightarrow Fe + Fe_2O_3 + O^{2-} \quad [5]$$

(a) (b) (c)

Fig. 4 Photos of Fe_2O_3 pellet (20 mm, ϕ10 mm, 5.5 g).
The quantity of the flowed electricity:
(a) Before electrowinning, (b) 15,000 (75%Q_0), and (c) 20,000 C (100%Q_0)

(a) (b)

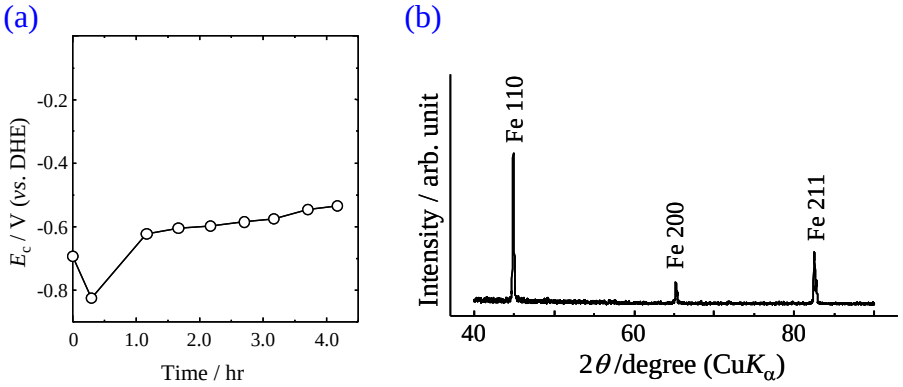

Fig. 5 (a) Time dependences of the cathodic potential during the electrowinning (1.0 A, 15,000 C) and (b) an XRD pattern of the pellet obtained after terminating electrowinning (1.0 A, 20,000 C) in 50 *wt*% NaOH-H_2O at 110°C.

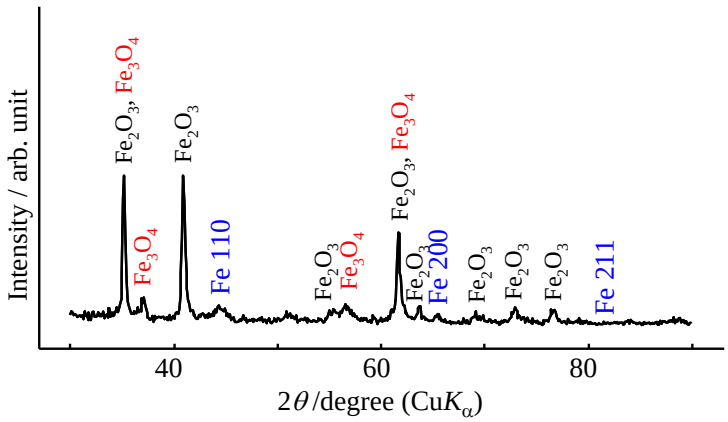

Fig. 6 An XRD pattern of the powder obtained after terminating electrowinning (0.6 A, 100,000 C) in 50 *wt*% NaOH-H_2O at 110ºC.

3.2 Suspension Electrolysis of Fe_2O_3 particle

The typical time dependencies of the cathodic and the anodic potentials during electrowinning at 40 *wt*% of the Fe_2O_3 particle concentration are shown in Figure 7. Both potentials of the cathode and the anode showed the stable values, which suggest that stable reactions progress at the electrodes. The cathodic potential (-0.18 V *vs*. DHE) was more positive value than the cathode limit (the hydrogen evolution) on graphite disk cathode in the 50 *wt*% NaOH-H_2O electrolyte (-0.28 V in Fig. 8a), which suggests that the Fe_2O_3 particle is directly reduced on the disk cathode. And also, the anodic potential (1.4 V) corresponds to the anode limit (oxygen evolution) in the NaOH-H_2O electrolyte (Fig. 8b).

Figure 9 shows the steady-state polarization curves at various Fe_2O_3 particle concentrations. The limiting current density increases by raising the rotation speed of the disk cathode due to promoting the convection-diffusion of the Fe_2O_3 particles in the electrolyte. At Fe_2O_3 particle concentration lower than

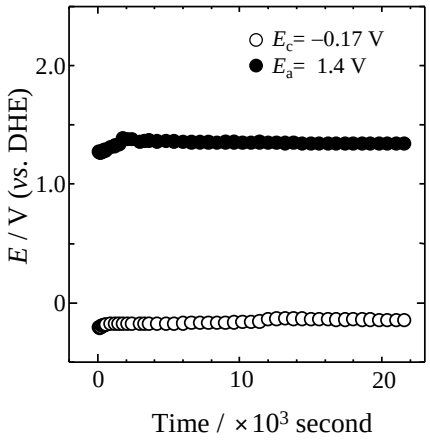

Fig. 7 Time dependences of the electrodes potentials during the electrowinning (1,000 A·m^{-2}, 1,000 rpm) in 50 *wt*% NaOH-H_2O+Fe_2O_3 (40 *wt*%) at 110˚C.

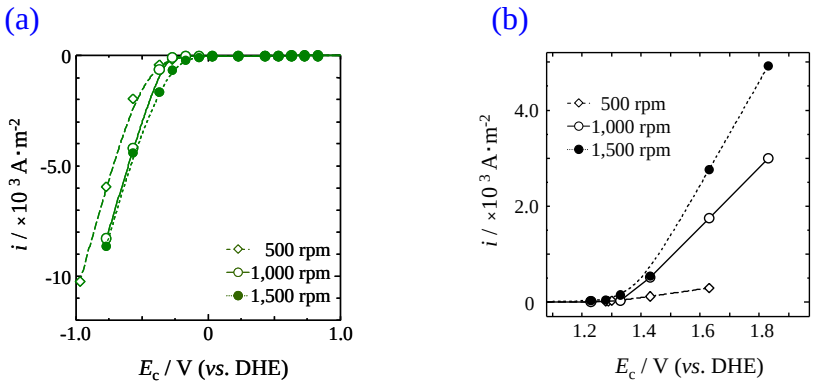

Fig. 8 Steady-state polarization curves in 50 *wt*% NaOH-H_2O at 110˚C.
(a) cathodic sweep and (b) anodic sweep

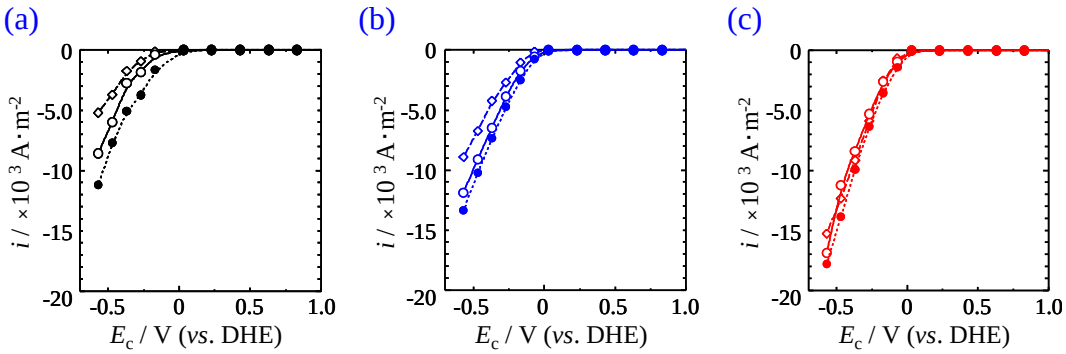

Fig. 9 Steady-state polarization curves at various Fe_2O_3 particle concentration in 50 *wt*% NaOH-H_2O+Fe_2O_3 at 110˚C.
Fe_2O_3 particle concentration: (a) 5.0, (b) 33, and (c) 40 *wt*%

33 *wt*%, the dependence of the polarization curve on the rotation speed of the disk was confirmed (Figs. 9a and b). In addition, polarization improved with increasing the concentration of the Fe_2O_3 particle. The solubility of the Fe_2O_3 in this electrolyte is 8.6×10^{-2} *wt*% at 140ºC [4] and is less than 5.0 *wt*% of the Fe_2O_3 particle. Therefore, the larger current at a higher Fe_2O_3 particle concentration is caused by promoting the convection-diffusion of the Fe_2O_3 particle, which confirms that the cathodic reaction progresses due to the direct reduction of the Fe_2O_3 particle according to reaction (1) in this process.
On the other hand, its dependence was greatly reduced at 40 *wt*% Fe_2O_3 particle concentration until 6,000 A·m^{-2}. This means that the transport of the Fe_2O_3 particle on the cathode surface is very fast at 40 *wt*% Fe_2O_3 particle concentration and the rate of the convection-diffusion of the Fe_2O_3 particle did not change until 6,000 A·m^{-2}.

Typical cyclicvoltammogram of Fe_2O_3 particle on graphite cathode in the NaOH-H_2O+Fe_2O_3 (40 *wt*%) are shown in Figure 10. In the anodic sweep, the oxidation behavior of Fe deposited on the cathode was observed in the NaOH-H_2O electrolyte. The anodic current was increased at around 1.5 V, which is corresponding to the oxygen evolution (in Fig. 8b).

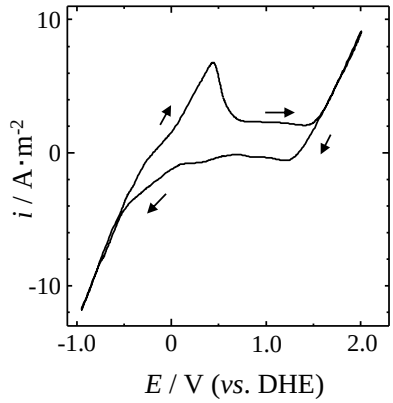

Fig. 10 Typical cyclicvoltammogram on graphite disk cathode (1,000 rpm) in 50 *wt*% NaOH-H_2O+Fe_2O_3 (40 *wt*%) at 110˚C. Scan rate: 100 mV/sec, 3rd cycle

These results confirmed that the anodic reaction is the oxygen evolution by reaction (6) during the electrowinning period.

$$2OH^- \rightarrow \tfrac{1}{2}O_2 + H_2O + 2e^- \qquad [6]$$

As for the cathodic sweep, the cathodic current was gradually increased at around 0 V, which is corresponding to the direct reduction of Fe_2O_3 particle on the surface of the cathode disk. The cathodic current was steeply increased since around -0.5 V due to start the hydrogen evolution.

The XRD patterns and SEM images of the film obtained on the disk cathode after terminating electrowinning at 40 and 33 *wt*% Fe_2O_3 particle concentrations are shown in Figs. 11 and 12. The XRD patterns show that these films were consisted of pure iron and that their crystallinity was changed by changing the current density. The morphology of the deposited Fe strongly depends on the current density. The homogeneous and smooth Fe films were obtained at 1,000 Am^{-2}, and heterogeneous Fe films were obtained by increasing the higher current density (~6,000 $A \cdot m^{-2}$). More homogeneous films were obtained at 40 *wt*% than 33 *wt*%. This tendency can be explained by their overpotential difference. The polarization difference between 40 and 33 *wt*% of Fe_2O_3 particle concentrations was larger with a high rotation speed of the disk cathode (Figs. 9 b and c). The high overpotential electrowinning forms the heterogeneous film and also leads to evolve the hydrogen. The current efficiency of reaction (1) according to Faraday's law is estimated from the weight of each obtained Fe film (Fig. 13). Fe films were obtained with current efficiency higher than 95% until 3,000 $A \cdot m^{-2}$ at 40 *wt*% Fe_2O_3 particle concentration, although the current efficiency decreased by a higher current density than 4,000 $A \cdot m^{-2}$. At the current density of 6,000 $A \cdot m^{-2}$, heterogeneous surface was spherically upheaved. Therefore, at a high current density, some electrodeposited Fe fall into the electrolyte due to the heterogeneous crystallinity and the current efficiency decreases. The morphology dependence of the electrodeposited Fe film on the electrolysis conditions is described in section 3.3.

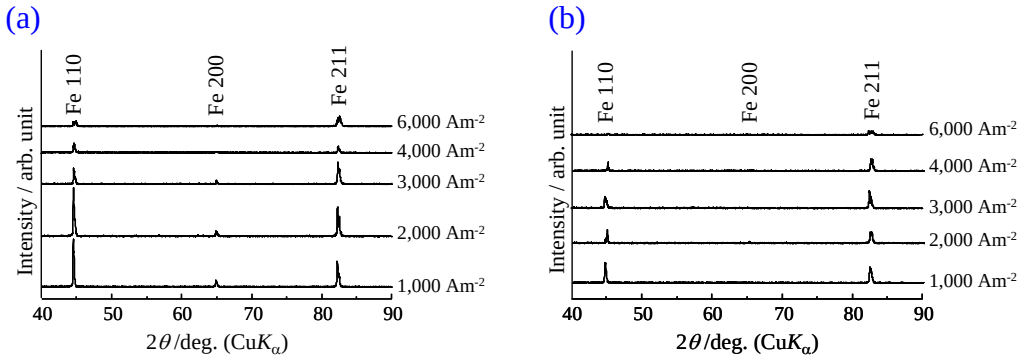

Fig. 11 XRD patterns of Fe films obtained on the cathode disk after terminating the electrowinning in 50 *wt*% NaOH-H_2O+Fe_2O_3 at 110˚C.
Fe_2O_3 particle concentration: (a) 40 and (b) 33 *wt*%

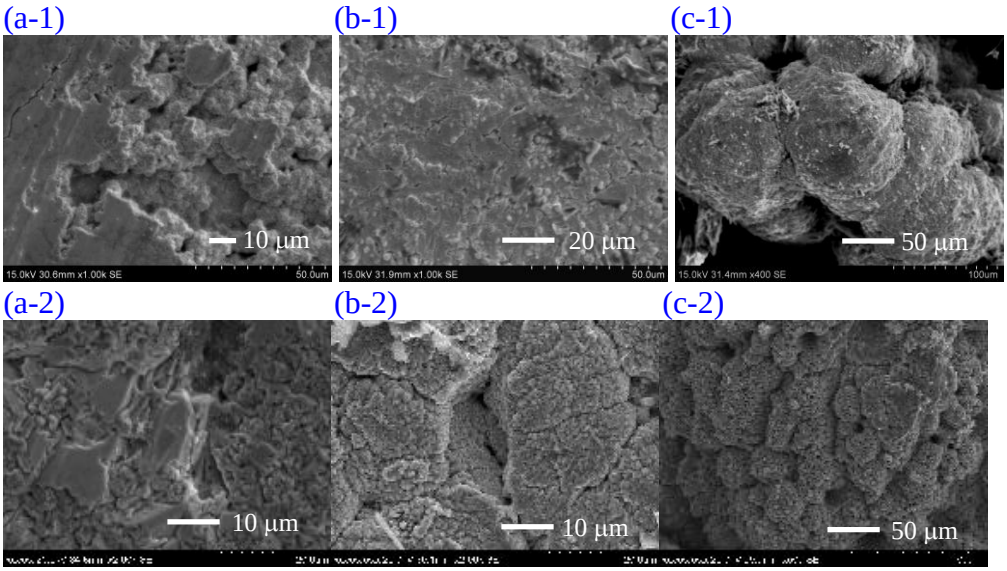

Fig. 12 SEM images of Fe films obtained on the cathode disk after terminating the electrowinning in 50 *wt*% NaOH-H_2O+Fe_2O_3 at 110˚C.
Current density: (a) 1,000, (b) 3,000, and (c) 6,000 $A \cdot m^{-2}$
Fe_2O_3 particle concentration: (1) 40 and (2) 33 *wt*%

3.3 Growth Process of Iron in Electrowinning Process

The SEM images of the Fe film obtained on the disk cathode after terminating electrowinning at 33 *wt*% Fe_2O_3 concentration are shown in Figure 14. The cubic α-Fe particle with the side length of around 0.1 μm was columnar-grown toward the specific direction. The dependence of the orientation index *M* on the current density estimated from Equation (2) is shown in Figure 15. The orientation index show that crystal orientation changes by increasing the current density (Fig. 15a). For the columnar-grown α-Fe particles, the (211) face plane of α-Fe was preferentially orientated. The dependence of orientation index *M* on the

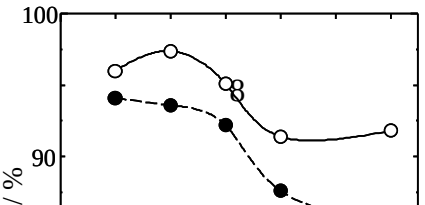

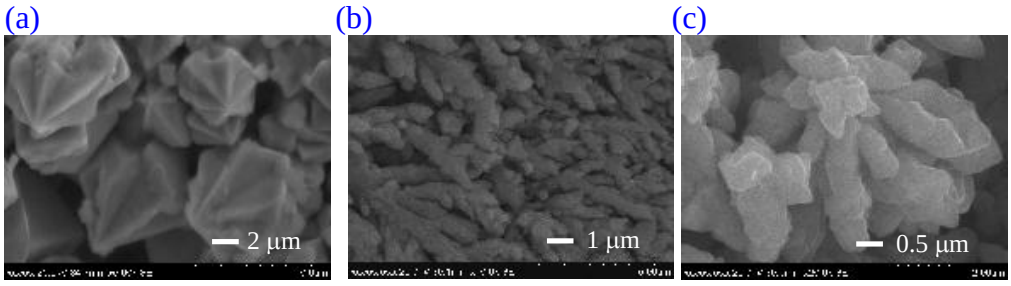

Fig. 14 SEM images of the surface of the iron deoxidated on the cathode disk after terminating electrowinning in 50 *wt*% NaOH-H_2O+Fe_2O_3 (33 *wt*%) at 110˚C. Current density: (a) 1,000, (b) 3,000, and (c) 6,000 A·m^{-2}

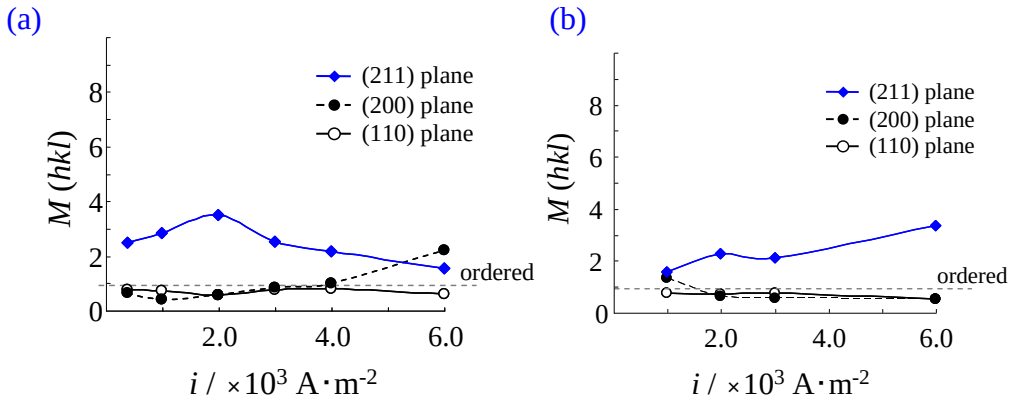

Fig. 15 Dependence of orientation index *M* on the current density. Fe_2O_3 particle concentration: (a) 33 and (b) 40 *wt*%

current density observed in this study agreed with the electrodeposited Fe from dissolved iron ions [8-11]. These results suggest that α-Fe particles grow by spiral dislocation according to two-dimensional nucleation theory [12-14]. Therefore, during electrowinning, the Fe_2O_3 particles receive the electrons on the cathode surface and are directly reduced while OH^- ions dissolve in the electrolyte. The deposited Fe atoms form the Fe phase on the surface of a Fe_2O_3 particle. After this, the grown Fe layer forms a cubic particle smaller than 0.1 μm. Taking into account the interface energy difference of each crystal face in the first neighbors for simplification, the interface energy γ of each crystal face is

$$\gamma_{110} = \frac{\sqrt{2}}{4a^2}\varepsilon, \quad \gamma_{200} = \frac{1}{2a^2}\varepsilon, \quad \gamma_{211} = \frac{\sqrt{6}}{3a^2}\varepsilon,$$

where ε is the work requirement for breaking a bond between first neighbors and a is the crystal constant of the α-Fe (bcc) crystal.
Therefore,

$$\gamma_{211} > \gamma_{200} > \gamma_{110}$$

These interface energy differences generate the anisotropy of growth direction due to the growth rate difference of each crystal face contributed by the activation energy difference. Therefore, the nucleated Fe is preferentially orientated toward the (211) face plane as the growth center.

At high current densities, the crystal also orientates toward the (200) crystal plane direction and heterogeneous films are obtained (Figs. 12c). These results are related to the transfer rate of the nucleated Fe to the growth center. Grujicic and Pesic [15] conducted Fe nucleation from the dissolved Fe ions and found that the Fe nucleus was nucleated by progressive nucleation. This result suggests that the growth of the Fe nucleus is extremely fast compared with the Fe nucleation in the ambient temperature region. At higher current density electrowinning, the nucleation becomes fast due to higher overpotential and the number density of the Fe nucleus increases. Here, when the transfer rate of the Fe nucleus to the growth center is late, Fe particle is grown on a growth plane other than the (211) face plane. Consequently, heterogeneous Fe film is obtained.

On the other hand, with 40 *wt*% Fe_2O_3 particle concentration, the Fe crystal nuclei orient toward the (211) face plane until 6,000 $A \cdot m^{-2}$ (Fig. 15b). The results of Figure 9 also suggest that the transport of the Fe_2O_3 particle for the cathode surface is very fast at 40 *wt*% of Fe_2O_3 particle concentration. Therefore, this might be caused by their difference of the transfer rate of the Fe_2O_3 particle. When the transfer of the Fe_2O_3 particle to the cathode is slow, the overpotential was increased. Then, the heterogeneous film was formed as above and the hydrogen was also evolved. At a high Fe_2O_3 particle concentration, the direct reduction of the Fe_2O_3 particle progresses on the cathode due to the fast transfer of the Fe_2O_3 particle to there. Thus, the transfer of the Fe nuclei is fast and the hydrogen is little evolved. This consideration agrees with the dependence of the average grain size of α-Fe on the current density (Fig. 16). At 33 *wt*% of the Fe_2O_3 particle concentration, the size of α-Fe crystal grain decreased by increasing the current density, despite of that the nucleation rate become to be fast due to increasing the overpotential. On the other hand, the grain size increased with

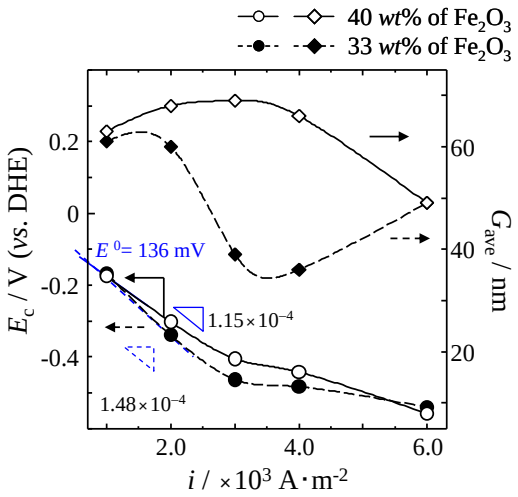

Fig. 16 Cathodic potentials and average grain sizes of Fe films obtained on the cathode disk after terminating the electrowinning at various current densities in 50 *wt*% NaOH-H_2O+Fe_2O_3 at 110˚C.

higher current density at 40 *wt*% of the Fe_2O_3 particle concentration (~3,000 A·m^{-2}). From these results, it was confirmed that the transfer rate of the Fe_2O_3 particle affects on the growth process of α-Fe crystal. These results suggest that the growth process of the deoxidated Fe depends on the transfer rate of the Fe_2O_3 particle.

4. Conclusion

Electrowinning of iron was conducted in a 50 *wt*% NaOH-H_2O electrolyte suspended Fe_2O_3 particle at 110ºC and pure α-Fe films were obtained on the disk cathode with a current efficiency higher than 95%. The Fe_2O_3 particle was directly reduced on the surface of the disk cathode and the deposited Fe atoms formed a cubic particle with a side length of around 0.1 μm. The crystal orientation of α-Fe depends on electrolysis conditions such as current density and Fe_2O_3 particle concentration, and the (211) face plane of α-Fe was preferentially orientated. Therefore, a cubic α-Fe particle columnar-grows toward the (211) face direction by spiral dislocation after 2D nucleation. In addition, the morphology of the obtained Fe films can be controlled by the current density and the transfer rate of the Fe_2O_3 particle concentration.

Acknowledgements

This study was supported by the Grant-in-aid from the IERO project. M. Tokushige was supported by the Grant-in-aid from the Oronzio and Niccoló De Nora Foundation Fellowship.

References

1. G.M. Haarberg, E. Kvalheim, S. Rolseth, T. Murakami, S. Pietrzyk and S. Wang, *ECS Transactions*, **3**, 341 (2007).
2. B. Yuan, O.E. Kongstein and G.M. Haarberg, *J. Electrochem. Soc*., **156**, D64 (2009).
3. A. Allanore, H. Lavelaine, G. Valentin, J. P. Birat and F. Lapicqueb, *J. Electrochem. Soc*., **155**, E125 (2008).
4. G. Picard, D. Oster and B. Tremillon, *J. Chem. Res., Synop.*, **8**, 252 (1980).
5. FACT Thermodynamics Database
6. K.V. Gow and G.J. Hutton, *Electrochimica Acta*, **17**, 1797 (1972).
7. K.E. Heusler and R. Knoedler, *Electrochimica Acta*, **15**, 243 (1970).
8. S. Yoshimura, S. Yoshihara, T. Shirakashim and E. Sato, *Electrochimica Acta*, **39**, 589 (1994).
9. S. Bodea, L. Vignon, R. Ballou and P. Molho, *Phys. Rev. Lett*., **83**, 2612 (1999).
10. H. Matsushima, T. Nohira, I. Mogi and Y. Ito, *Surface and Coatings Technology*, **179**, 245 (2004).
11. H. Matsushima, T. Nohira and Y. Ito, *Electrochem. Solid-State Lett*., **7**, C81 (2004).
12. N.A. Pangarov, *Electrochimica Acta*, **7**, 139 (1962).
13. N.A. Pangarov, *J. Electroanal. Chem*., **9**, 70 (1965).
14. N.A. Pangarov and S.D. Vitkova, *Electrochimica Acta*, **11**, 1719 (1966).
15. D. Grujicic and B. Pesic, *Electrochimica Acta*, **50**, 4405 (2005).